


Article

Kinetic Model Evaluation of Arsenic and Selenium Sources in Waste Rock of the Powder River Basin, USA

Jeff B. Langman 

Department of Earth and Spatial Sciences, University of Idaho, Moscow, ID 83844, USA; jlangman@uidaho.edu; Tel.: +1-208-885-0310

Abstract: Groundwater quality can be impacted by the backfilling of coal pits with waste rock containing new mineral surfaces and nanomaterials. This study was implemented to identify newly available arsenic and selenium sources in waste rock from the Cordero Rojo Mine in the Powder River Basin, Wyoming, to highlight the alteration of contaminant sources with the transition from an overburden geologic state to the mined waste rock. Basic kinetic models were constructed to replicate the possible weathering modeling scenario derived from published sources of arsenic and selenium in the Powder River Basin overburden—pyrite and gypsum, respectively. These basic prediction models were unable to capture the arsenic and selenium trends recorded for a saturated column loaded with waste rock from the Cordero Rojo Mine. Enhanced kinetic models were tested through trial and error to capture newly available sources created by the mining of the waste rock. The incorporation of new source contributions produced modeled arsenic and selenium trends similar to the observed trends in water extracted from the column. The identification of newly available contaminant sources in backfill waste rock is necessary to evaluate the potential release of contaminants and the exceedance of water quality criteria for overburden formations that have not previously shown the potential for water quality contamination.

Keywords: waste rock weathering; nanomaterial generation; contaminant modeling



Citation: Langman, J.B. Kinetic Model Evaluation of Arsenic and Selenium Sources in Waste Rock of the Powder River Basin, USA. *Mining* **2024**, *4*, 469–488. <https://doi.org/10.3390/mining4030027>

Academic Editors: Mostafa Benzaazoua and Yassine Ait-Khouia

Received: 19 April 2024

Revised: 1 July 2024

Accepted: 5 July 2024

Published: 12 July 2024



Copyright: © 2024 by the author. Licensee MDPI, Basel, Switzerland. This article is an open access article distributed under the terms and conditions of the Creative Commons Attribution (CC BY) license (<https://creativecommons.org/licenses/by/4.0/>).

1. Introduction

Post-mining remediation can include waste rock backfilling of open pits, which creates aquifer matrices that are substantially different from the surrounding aquifer. Not only is the physical structure of the waste rock different from its original geologic state, but new mineral surfaces and easily weathered nanomaterials (e.g., very fine to ultrafine dust particles) have been created that may impact water quality during and after groundwater recovery [1–3]. Particle generation from mining, particularly open pit mining, can generate substantial and transportable particles that are traditionally viewed as air pollutants (fugitive dust) [4] but also have the potential to influence water resources because of their higher reactivity (e.g., high surface-to-volume ratio) and transportability during weathering. The alteration from a geologic state to a post-mining, waste-rock fill that has been cut, blasted, hauled, dumped, and graded creates potential new contaminant sources that were previously unavailable, or had limited availability, in the original geologic state [5–8]. With groundwater recovery in a newly constructed backfill aquifer, a high and variable solute load may propagate through the aquifer (Figure 1) as new mineral surfaces and nanomaterials are exposed to weathering processes [9–14]. The potential for increased mineral reactivity (e.g., fresh mineral surfaces or nanomaterials) and variable release of solutes may produce conditions that are difficult to predict with hydrogeochemical models using existing knowledge of the overburden/waste rock formations [15–17].

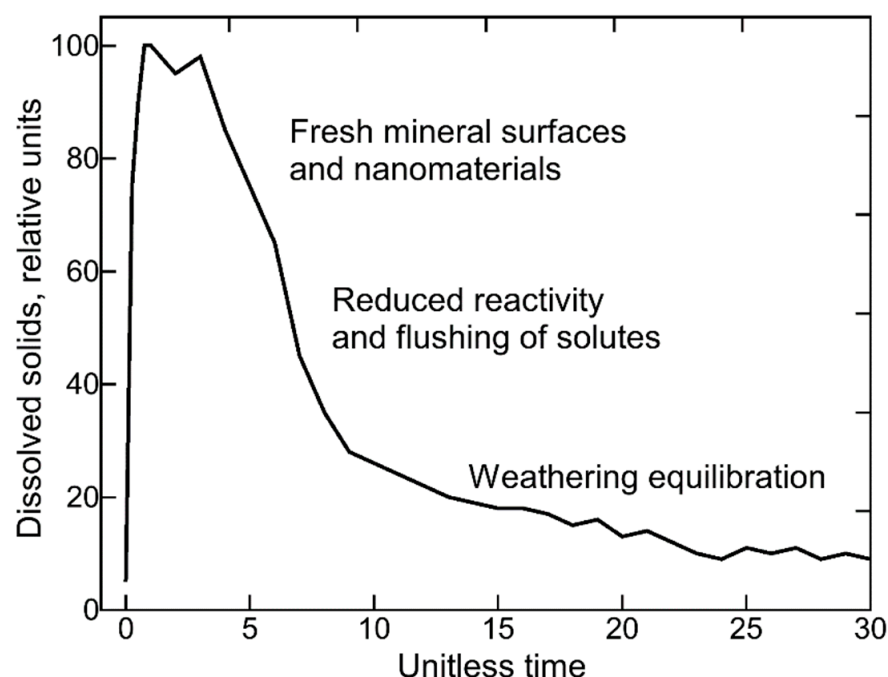


Figure 1. Possible trend of solute release with weathering of fresh waste rock (modified from Langman et al. [18]).

Coal mine waste rock (spoils) refers to low-grade ore and rock units overlying and interbedded with economically viable coal layers. Commonly, this waste rock is stored and then backfilled into the excavated areas as spoil dumps, which become backfill aquifers with groundwater recovery. The hydrologic characteristics of the backfill aquifer will vary depending on the method of mining, backfill placement/compaction, backfill composition, and particle size distribution [19]. Excluding recharge and flow variability in the backfill aquifer, the release of contaminants such as arsenic [As] and selenium [Se] from waste rock will be determined by the availability and reactivity of their mineral sources that likely were altered with mining [20–22]. If substantial new mineral surfaces and nanomaterials were generated with mining, these new sources can result in a quicker contaminant release and poor water quality during the initial weathering stage [23–26]. Water quality impacts (exceedance of regulatory criteria) have been documented for up to 15+ years in backfill aquifers in the Powder River Basin, Wyoming, USA (Figure 2) [9], where groundwater extracted from the unmined overburden typically does not have water quality issues. The length of this stage of poorer water quality with the initial weathering of the backfill is dependent on weathering rates and the amount of newly exposed mineral surfaces and nanomaterials generated from mining [18,27–31].

Coal mining in the Powder River Basin, the largest coal mining region in the USA, includes the removal of a sedimentary overburden that is temporarily stored before landscape reconstruction (Figures 3 and 4). Surface water and shallow groundwater in the Powder River Basin have shown exceedance of water quality criteria for As and Se at select times and locations, which are attributed to coal mining and waste rock backfilling [32–36]. Waste rock derived from the overburden at the Cordero Rojo Mine in the Gillette Coal Field of the Powder River Basin (Figure 2) is composed of the Wasatch and Fort Union formations—sequences of interbedded fluvial, lacustrine, and palustrine deposits [37–39]—that typically do not produce groundwater with elevated As or Se concentrations [40,41]. The blasting and transport of the overburden waste rock produces new mineral surfaces and nanomaterials that may increase the availability of potential contaminants such as As and Se [11,20,27,42,43]. Transport of nanomaterials (at least one dimension at the nanometer scale [10]) also can contribute to the solute load through inclusion in the dissolved solute phase (< 450 μm filtering) [14] of groundwater migrating through the backfill aquifer. The goal of this study was to evaluate

potential new sources of As and Se in the waste rock through a comparison of kinetic (forward or predictive) models and kinetic column results from the weathering of the waste rock from the Cordero Rojo Mine. The output of the mineral weathering models is used to highlight the difficulty of predicting waste rock weathering from known contaminant sources present in the geologic state of the overburden.

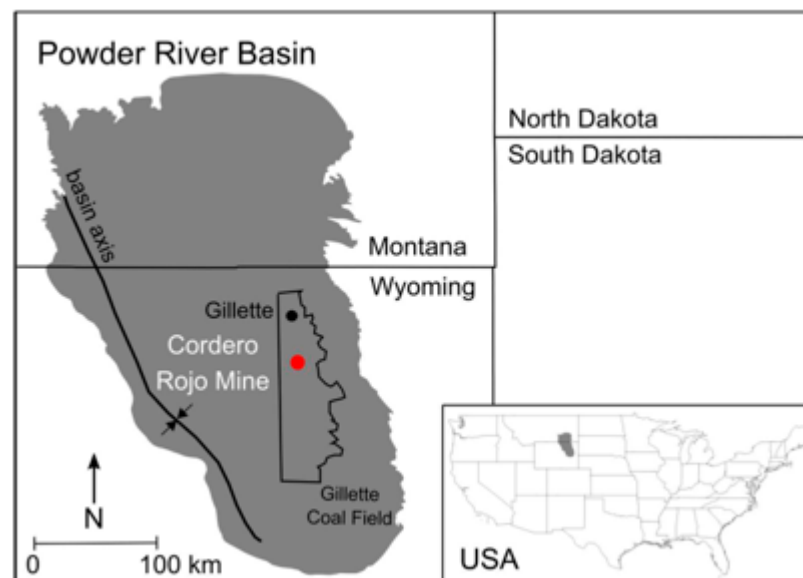


Figure 2. Powder River Basin, Gillette Coal Field, and Cordero Rojo Mine, Wyoming, USA (modified from Martin and Langman [31]).



Figure 3. Removal of overburden and waste generation during open-pit coal mining at the Cordero Rojo Mine, Powder River Basin, Wyoming, USA (Martin and Langman [31]).



Figure 4. Reconstructed landscape adjacent to the active Cordero Rojo Mine, Powder River Basin, Wyoming, USA. The coal pit has been filled with waste rock (backfill), graded, and covered with seeded topsoil along with reconstruction of water features.

1.1. Powder River Basin Waste Rock

Waste rock from the Cordero Rojo Mine is representative of the overburden for coal mines in Gillette Coal Field, Wyoming, where open pit mines form the most prolific coal mining region in the USA. The overburden consists of the siliciclastic Wasatch and Fort Union formations (Figure 5) [44]. The waste rock derived from the overburden is composed primarily of low-reactivity minerals (Supplementary Materials) (e.g., aluminosilicates) derived from sequences of interbedded fluvial, lacustrine, and palustrine deposits [37–39]. These formations contain sandstone with smaller amounts of limestone and relatively non-sulfidic mudstones (primarily phyllosilicate clays such as smectite, vermiculite, kaolinite, illite, and chlorite) [37] whose paleoenvironments produced the low sulfur (typically < 1% [45]) coal found in this region [46–48]. The overburden that must be removed for mining the coal (Figure 5) produces large waste piles (Figure 3) that are later deconstructed and reworked during landscape reconstruction (Figure 4). Removal of the overburden produces a waste rock with small amounts of coal and a very large grain size distribution (clay to boulder, Figure 6). A grain size distribution analysis for the < 6.3 mm waste rock samples used in the column study [31] indicated a greater fraction of clay-sized particles in the Fort Union sample compared to the Wasatch sample, which translated to a greater surface area of 14.2 m²/g for the Fort Union sample compared to the 5.1 m²/g for the Wasatch sample.



Figure 5. Overburden and coal seam at the Cordero Rojo Mine, Powder River Basin, Wyoming, USA (Martin and Langman [31]).



Figure 6. View of the particle size variability in waste rock generated at the Cordero Rojo Mine in the Powder River Basin, Wyoming, USA. Waste rock can range from clays to boulders.

1.2. Arsenic and Selenium Sources

Weathering of the Wasatch and Fort Union waste rock is not expected to release substantial As and Se because of the lack of these elements in regional groundwater extracted from these formations [41]. Yet, backfill aquifers in this region have shown As and Se concentrations exceeding water quality criteria [49]. Dissolution of salts that were previously unavailable to groundwater in the overburden and the oxidation of contaminant-bearing minerals associated with the coal have been hypothesized as the likely sources of As and Se [9,35,50–52]. This perception of potentially no impact on groundwater quality from backfill aquifers and multiple hypothesized sources of As and Se is the basis of this study's question regarding new mineral surface availability, generation of contaminant-containing nanomaterials, and the need to identify such sources for prediction of future groundwater quality. Removal of the overburden during mining can produce a wide range of particle sizes (Figure 5), but it is the exposure of new mineral surfaces and the generation of the nanomaterials that can produce high weathering rates and the substantial release of potential contaminants [11,20,23,27,42,53,54]. The generation of nanomaterials also produces particles that can be electrostatically sorbed to the larger bulk solids, which can readily desorb and be transported with infiltrating water [53,55–58].

Powder River coal is relatively low in As (median 1.9 ppm) compared to more As-rich coal from Appalachia (8 to 29 ppm) and the Western (14 ppm) and Eastern (10 ppm) Interior [59]. Iron sulfides such as pyrite [FeS₂], and arsenides such as loellingite [FeAs₂], can be hosts for As in such geologic environments [60]. Arsenic has been detected in the Fort Union Formation, which contains the deltaic deposits that produced the sulfides and the mined Wyodak-Anderson coal seam of the Tongue River Member [37,61]. The As can be found sorbed to iron- and manganese-oxides [61], in pyrite (e.g., As-bearing pyrite), and, to a lesser extent, in organic portions of the coal [59]. As-bearing pyrite is a common source for the release of As with weathering of mine waste [62], and nanoparticle pyrite (nanopyrite) has been found in coal mine waste rock along with associated substitution elements such as As [63,64]. During groundwater recovery, the oxidative dissolution of newly exposed As-bearing pyrite could release soluble As³⁺ and As⁵⁺ complexes [65]. Given the known As association with pyrite and the incorporation of small amounts of pyrite-containing coal in the Cordero Rojo waste rock, the release of As from the weathering of the waste rock can be modeled by the oxidative dissolution of As-bearing pyrite [66].

Selenium is typically found in the environment as selenide (H₂Se, HSe[−]), selenium (Se⁰), selenite (SeO₃^{2−}), or selenate (SeO₄^{2−}), depending on the pH and redox conditions during deposition [67]. Selenite and selenate will be the dominant forms available as potential solutes, but selenite typically will sorb to particles, particularly iron (oxyhydr)oxides, while selenate is soluble and mobile because of its weak sorption to particles [68]. Within the Powder River Basin, Se is found in the coal, in coal-associated pyrite or other sulfides, in water-leachable salts, and sorbed to particles [69]. Dreher and Finkelman [35] indicated that Se salts from past oxidation of pyrite may be the primary source of Se in the Powder River Basin overburden. Sharmasarkar and Vance [70] found Se strongly correlated with clay fractions in Powder River Basin overburden formations. Selenium salts readily dissolve, but the dissolution of Se salts may not contribute substantial soluble Se species (e.g., HSeO₃[−] or SeO₄^{2−}) if selenite is produced, given its preference to readily sorb to sediments [71–74]. For the weathering of Powder River Basin waste rock, Se can be modeled as the dissolution of Se-containing gypsum [CaSO₄]. The incorporation of Se into gypsum would be expected (Se is a common substitute for S), given the past oxidation of pyrite and coal as indicated by the significant presence of gypsum in Powder River Basin sedimentary formations [49,75–78].

1.3. Kinetic Modeling

Simplified predictive (kinetic reaction) mineral-weathering models were created with PHREEQC 3 for As and Se release from the Cordero Rojo waste rock based on the perceived sources in the overburden formations (e.g., pyrite and gypsum). Such models represent

the likely predictive element-release tool that could be derived from the available information for estimating potential impacts on groundwater quality with weathering of known contaminant-containing sources that were present in the overburden and now present in the waste rock. The model application used PHREEQC's capability to simulate the dynamic process of reaction kinetics (e.g., RATES and KINETICS code blocks for mineral weathering) to reflect the contributions of the contaminant sources within the waste rock. Enhanced predictive models were constructed to account for new mineral surfaces and the generation of nanomaterials, given the substantial alteration of the overburden during mining. The goal was to compare typical mineral-weathering models built around As and Se release from known sources to enhanced models focused on replicating the contribution from the weathering of newly available sources generated from the mining process.

2. Materials and Methods

To evaluate the application of the kinetic models for estimating the potential release of As and Se from the waste rock, a saturated column experiment was conducted to provide a temporal trend of the release of As and Se from fresh waste rock collected from the Cordero Rojo Mine. Availability of the As and Se temporal trends from the water extracted from the column allowed for the identification of possible additional sources of these contaminants that were not considered in the basic predictive models derived from a review of the literature regarding As and Se sources in the overburden formations. The use of the models and comparison between the basic and enhanced model outputs is not to create predictive models for future waste rock analysis but to evaluate the As and Se source alteration from the overburden geologic state to the mined waste rock state. This evaluation highlights the difficulty in using published sources of the contaminants in the geologic state to determine potential water quality impacts.

2.1. Collection of Waste Rock for the Column Experiment

Waste rock samples of the Wasatch and Fort Union formations were collected within 2 weeks of initial excavation from the Cordero Rojo Mine in the Powder River Basin. Samples of the waste rock generated from the Fort Union and Wasatch formations were separately collected (the two types are segregated during mining) through a random selection method per standard practice for sampling aggregates [79,80] and screened to < 6.3 mm in the field [81–83].

2.2. X-ray Analysis of Arsenic and Selenium Sources

Wasatch and Fort Union waste rock were evaluated for major and minor element concentration by X-ray fluorescence (XRF) at the Washington State University GeoAnalytical Laboratory (Advant'XP+ sequential XRF, fused beads). Additionally, samples of Fort Union and Wasatch waste rock were examined by scanning electron microscope (Zeiss Supra 35 Variable-Pressure FEG SEM with Noran System Six EDS) at the University of Idaho Electron Microscopy Center to confirm potential sources of As and Se indicated by existing literature and to evaluate potential new sources derived from the mining process. Given the expectation of As association with pyrite in coal particles incorporated into the waste rock during overburden removal, an additional Fort Union sample was screened for coal particles by flotation for SEM analysis. For this flotation separation, 75 g of Fort Union waste rock was placed in a 1-L beaker with 500 mL of deionized water and agitated with an orbital shaker for 2 h. Approximately 2 g of coal particles floated to the water surface and were collected and inserted into a lyophilizer for 24 h.

2.3. Column Experiment

A 20-week, kinetic column experiment was conducted to evaluate the temporal trend of the release of As and Se from newly available sources in the waste rock collected at the Cordero Rojo Mine [31]. A warm-room (20 ± 1 °C), 0.6 m (H) \times 0.1 m (W) PVC column was loaded with 0.8 kg of Wasatch waste rock and 3.2 kg Fort Union waste rock to mimic the

overburden distribution at the Cordero Rojo Mine, which is replicated during landscape reconstruction. The weathering cycle for the column consisted of a twice-weekly schedule of the drip introduction of 1-L of deionized water and full saturation of the waste rock for 72 h, followed by a 2-h drain period (minimal disturbance of the waste rock with a $K < 10^{-5}$ m/s) and a 6-h unsaturated period before re-saturation of the column. This is a modification of the standard humidity cell protocol [83,84] to simulate saturated (e.g., aquifer) conditions and allow for the collection of sufficient water volume for analysis of environmental parameters and solutes [31]. The twice-weekly collection of water from the column was analyzed for pH (± 0.01 pH), Eh (± 0.2 mV), and specific conductance (± 0.01 $\mu\text{S}/\text{cm}$) with calibrated Orion 3-Star meters/probes and analysis of As and Se as unfiltered, 0.45- μm filtered, and 0.20- μm filtered samples. The As, Se, and additional elements, such as Fe, were determined by inductively coupled plasma optical emission spectrometry (ICP-OES) for larger concentrations (Perkin Elmer Optima 8300 ICP-OES) and inductively coupled plasma mass spectrometry (ICP-MS) for smaller concentrations (Agilent 7800 ICP-MS) at the University of Idaho Analytical Services Laboratory. Greater detail of the column experiment is presented in Martin and Langman [31], which describes an evaluation of column solute trends for field parameters and high-concentration solutes released from the waste rock.

2.4. Particle Size and ζ Potential

Immediately after sample collection, unfiltered column water was measured for particle size distribution and ζ potential, using a Brookhaven NanoBrook ZetaPALS. Samples were analyzed by dynamic light scattering for particle size distribution in water at 25 °C with a viscosity of 0.89 cP, a refractive index of 1.33, at a scattering angle of 90°, a dielectric constant of 78.54, a laser wavelength of 659 nm, and inputted pH and conductivity values. Analysis of ζ potential was performed as laser Doppler electrophoresis (phase analysis light scattering). The laser beam was passed through the sample undergoing electrophoresis, and the scattered light from the moving particles was frequency shifted, from which the electrophoretic mobility ($\text{m}^2 \text{V}^{-1} \text{s}^{-1}$), U , was determined given the laser wavelength and the scattering angle. The ζ potential was calculated from the electrophoretic mobility using the Smoluchowski solution ($\zeta = \mu U / \epsilon$), where ϵ is the electric permittivity of the solution ($\text{C}^2 \text{N}^{-1} \text{m}^{-2}$) [85].

2.5. Kinetic Models and Parameters

Four mineral-weathering models were constructed with PHREEQC: (1) As-bearing pyrite oxidation, (2) As-bearing pyrite oxidation + nanomaterial contribution, (3) Se-bearing gypsum dissolution, and (4) Se-bearing gypsum dissolution + nanomaterial contribution. Each model combined a well-oxygenated (pe of 12.5), near-neutral water (pH of 6) at 20 °C (replicative of column (ultrafiltration) water) with the likely As and Se sources found in the Wasatch and Fort Union formations. The column experiment resulted in a near-neutral, oxidizing environment throughout the experiment period [31], and the similar pH and oxidizing condition (not rate limited) of the model environment would not alter solute release over the model time period. To compare column and model results, the model As and Se outputs represent a total solution concentration.

The initial (basic) kinetic models (no nanomaterial source) were built on geochemical reactions of the bulk solid source of each of the contaminants—As-bearing pyrite (95% pyrite + 5% loellingite [FeAs_2]) and Se-bearing gypsum (95% gypsum + 5% nestolaite [CaSeO_3]). Arsenopyrite was not chosen for the oxidation reaction because it has not been identified in Powder River Basin coal and is structurally different (monoclinic and prismatic) compared to As-bearing pyrite (pyrite = cubic and diploidal + loellingite = orthorhombic and dipyrmidal). The available amounts of the As-bearing pyrite and Se-bearing gypsum were set to the total release of As or Se from weathering during the column experiment to align output scales for comparison of the temporal trends of the model outputs and the column results. These batch model simulations (no transport incorporated)

were aligned with the associated interval of new water inputs to the column experiment. The initial models represent the likely mineral-weathering modeling for the prediction of water quality impact from the generation and weathering of the waste rock given known information about the overburden material.

The initial As model was established as the oxidative dissolution of the As-bearing pyrite based on parameters described by Williamson and Rimstidt [86], which has a log k of -8.19 for pyrite. The initial Se model was established as the simplified dissolution of a dissolvable salt (log $k = -7$ for gypsum) given an initial area (A_0) to volume (V) ratio of 1.67 and an initial molar concentration (m_0). This simplified reaction rate removes concerns regarding surface area availability and roughness, while conveying the likelihood of the substantial dissolution of the gypsum following the production of the waste rock, which can produce very small and roughened particles but still retains partially bound (limited surface availability because of incomplete liberation) mineral forms that lessen reactivity [87]. The saturation index of gypsum was not incorporated into the reaction rate (negative feedback) given the limited amount of reacted gypsum (no saturation of the mineral phase). These parameters and reaction rate were evaluated against the column results to determine the applicability of the model parameters for replicating the initial reaction and mineral release of Se (dominant surface reaction as opposed to a surface-diffusion reaction [88]) that was expected during the early weathering stage of the column experiment. Enhanced models were constructed through trial and error of additional As or Se sources to produce a trend similar to the column output. The goal of the enhanced models was to identify potential source types that deserve consideration for predictive modeling of fresh waste rock where the act of mining has increased the availability of the target elements.

3. Results and Discussion

3.1. Arsenic and Selenium Source Identification

The XRF analysis of the waste rock indicated 7 ppm of As in the Fort Union sample and 2 ppm in the Wasatch sample (Se was not part of the XRF analysis). Examination of the waste rock with the SEM-EDS (examples shown in Figures 7 and 8) indicated the presence of As in coal particles (Fort Union sample) and distributed concentrations of Se (0.5 wt. %) in areas with high clay content (Fort Union and Wasatch samples). Analysis of the floated coal particles from the Fort Union waste rock indicated that As was consistently present in trace amounts (0.1 to 0.6 wt. %) throughout the coal particles, and Se was detected (up to 7 wt. %) as clay particles sorbed to larger particle surfaces. Results suggest a coal source for As and sorbed or precipitated Se particles with a greater abundance of both elements in the Fort Union waste rock.

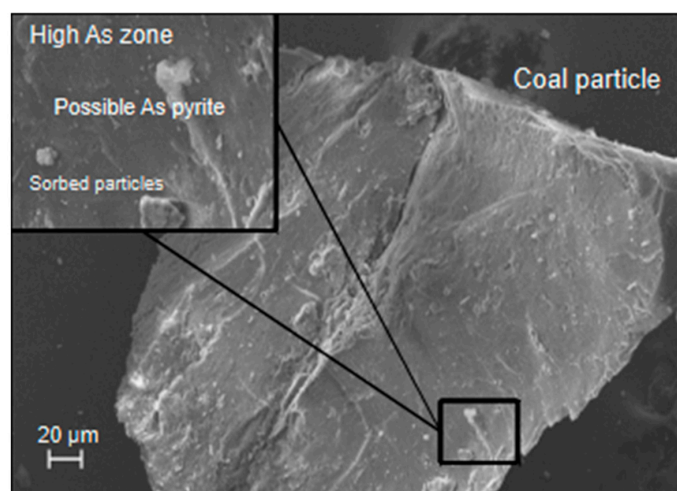


Figure 7. The likely presence of arsenic [As] as arsenic-bearing pyrite and sorbed particles on a pre-experiment coal particle from the Fort Union waste rock.

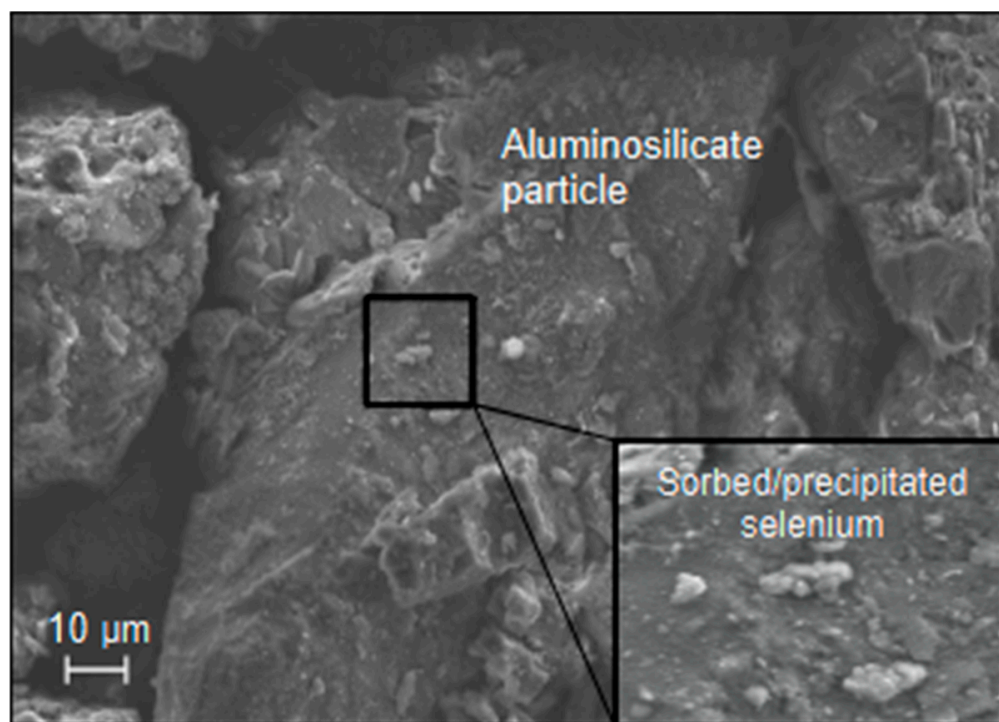


Figure 8. The likely presence of a sorbed selenium particle (e.g., selenite [SeO_3I]) on pre-experiment aluminosilicate (e.g., plagioclase) particle in the Fort Union waste rock.

3.2. Waste Rock Column Arsenic and Selenium Release

The release of As and Se from the waste rock in the column experiment was part of the release of the larger solute body [31] that produced a typical weathering trend (Figure 1) as indicated by a quick and early peak in specific conductance followed by a slower decrease until Day 40 and a final stage of apparent steady-state weathering (Figure 9). The As release was reflective of the assumed oxidative dissolution of As-bearing pyrite, with a slow increase in concentration until Day 20, followed by a slower decline in concentration reflective of the consumption of the available pyrite (Figure 9). Selenium release consisted of a quick peak at Day 3 and a slightly slower decline until Day 20, after which Se was no longer detected in the column water (Figure 9). The substantial difference in As and Se concentration trends is not unexpected given the likely association of As with pyrite [89] and Se in salts [31,32,35,41]. Some of the As trend represents the oxidation of the sulfide surface (shrinking core model of sulfide weathering [28,90–94]), which is controlled by the inward diffusion of oxygen given the blocking effect of Fe and S precipitates [95]. The quick release of Se indicates the likely dissolution of Se salts or desorption of Se-bearing particles, followed by the flushing of remaining Se-bearing particles and the continuing contribution from Se salt dissolution. Some of the released As and Se occurred as nanoparticles as indicated by particle size analysis (Figure 10). Large particles (mean > 3000 nm) were initially flushed from the column during the first week, followed by mean particle sizes in the 100 to 300 nm range until after Day 60 when the mean particle size increased to near 400 nm, then decreased. The associated ζ potential values varied between negative and positive values during the first 70 days reflective of the higher solute period where the greater reactivity of the mineral sources produced a range of cationic and anionic particles. The mean particle size in the column water increased after Day 90 until plateauing after Day 110, and the ζ potential remained positive during this period.

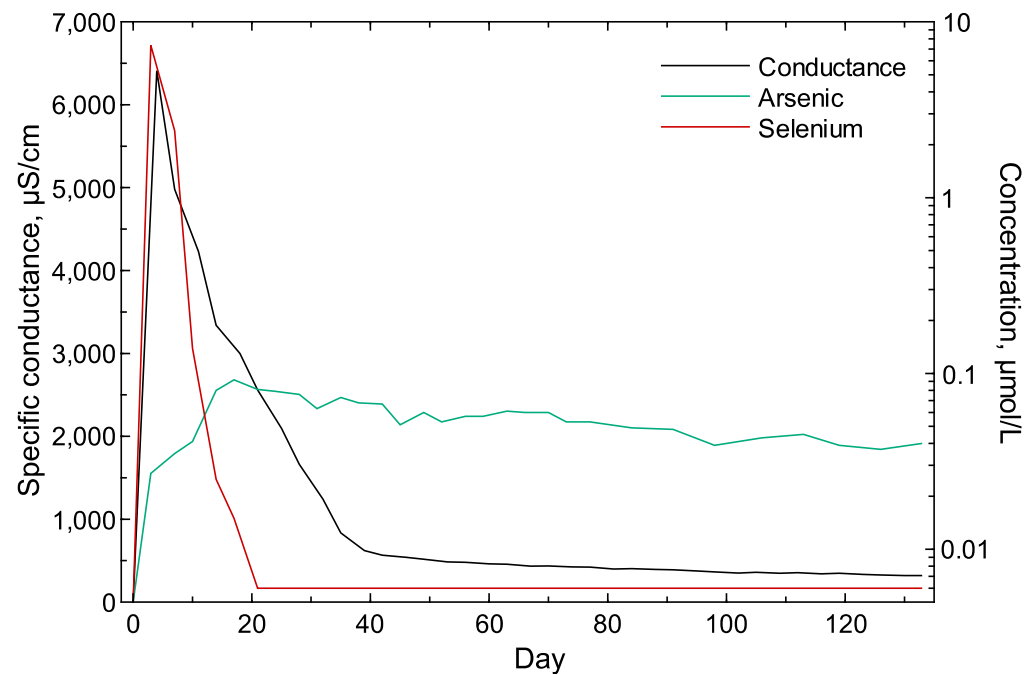


Figure 9. Specific conductance and total (unfiltered) concentrations of arsenic and selenium in the in water collected from the kinetic column containing the waste rock from the Cordero Rojo Mine. Non-detected selenium concentrations were set to 0.006 $\mu\text{mol/L}$ (half the reporting limit).

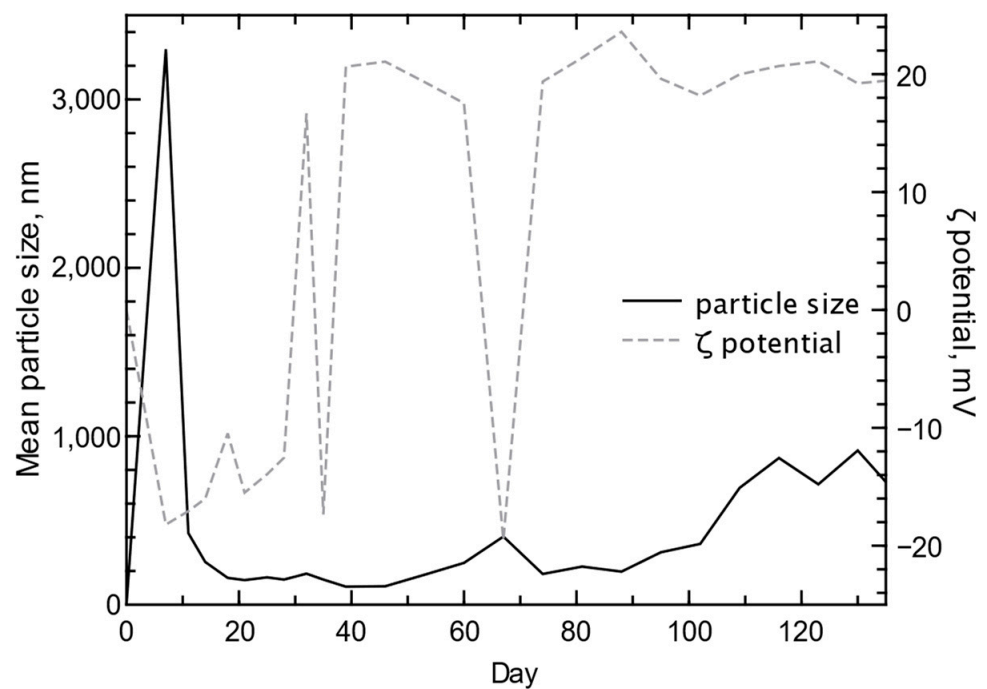


Figure 10. Mean particle size and ζ potential of water collected from the kinetic column containing the waste rock from the Cordero Rojo Mine.

3.3. Initial Arsenic Model vs. Column Experiment

The initial or basic As model did not produce an output trend similar to any of the As trends (unfiltered or filtered) from the column experiment (Figure 11). The model produced an As trend that would be expected from unweathered, As-bearing pyrite with a relatively quick peak followed by a slow decline in concentration. The unfiltered and filtered As concentrations recorded during the column experiment indicated an initial

peak (or shoulder) followed by a larger peak before a substantial drop in As release near Day 20 (unfiltered) or Day 24 (filtered values). The unfiltered As trend is more variable compared to the filtered As trends, likely because of larger particles moving through the column. The two-peak release (shoulder and main peak) in the As trend likely occurred because of multiple source contributions, such as initial nanoparticle flushing (no differences in unfiltered or filtered As concentrations during the first week) and the subsequent degradation of the bulk sulfide mineral source with oxidative dissolution of As-bearing pyrite.

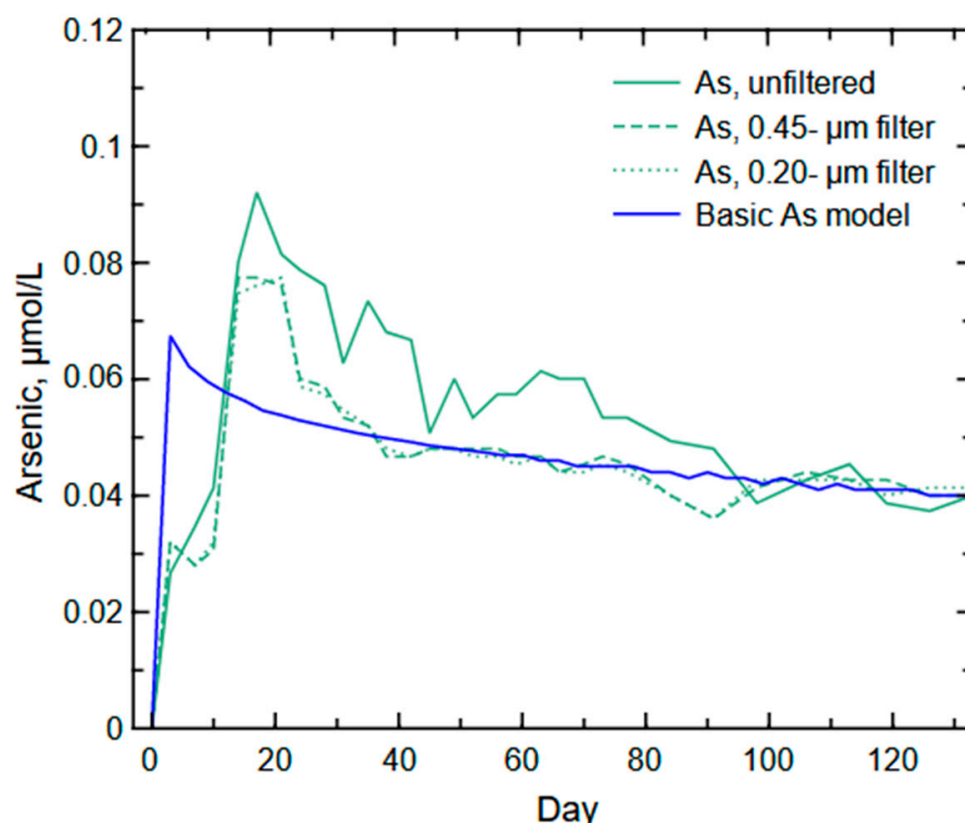


Figure 11. Arsenic results for the basic arsenic model with oxidative dissolution of arsenic-bearing pyrite and total (unfiltered) and filtered arsenic concentrations from the column experiment.

The delay in As release from the column waste rock likely is a result of the multi-step release of As from pyrite, where As is initially released from the degrading mineral as a non-soluble species (As^{3+} or AsO_3^{-3}) that will be sorbed before full oxidation to the more soluble As^{5+} or AsO_4^{-3} [96,97]. Arsenic released from the pyrite mineral structure can be retained by co-precipitation (e.g., ferric arsenates) and adsorption to Fe (oxyhydr)oxides that slow As release into solution [98]. Additionally, Cen et al. [97] found that the release of As^{3+} from the oxidative dissolution of arsenopyrite decreases with the presence of biochar, a similar inorganic/organic carbon form to coal. Such factors indicate the likelihood of the limiting of As release until full oxidation of the element and degradation or transport of sorbing surfaces. Therefore, the weathering processes for explaining the dual peak visible in the As released during the column experiment likely are an initial transport of As-bearing nanoparticles (e.g., sorbed to Fe (oxyhydr)oxides or As-bearing nanopyrite) followed by the greater release of As with the oxidative dissolution of the bulk As-bearing pyrite, and a subsequent slow decline as the sulfide mineral surface is decreased with further weathering.

3.4. Enhanced Arsenic Model vs. the Column Experiment

The weathering regime to be tested with the enhanced As model is the meshing of nanomaterial contribution and bulk solid weathering to capture the two-peak trend identified in the column results (Figure 11). An examination of the release of Fe during the column experiment indicates a similar trend of two peaks during the first 30 days of the column experiment (Figure 12). There appears to be a flushing of Fe-bearing particles that may be carrying As. The range of particle sizes (e.g., nanoscale to microscale) were large given the filtered Fe concentration was substantial during the first peak (0.06 $\mu\text{mol/L}$) compared to the total Fe concentration (0.07 $\mu\text{mol/L}$) and the mass of As ($\sim 0.03 \mu\text{mol/L}$ in the total and dissolved concentrations). The initial peak of As and Fe likely is the result of the flushing of mostly nanoparticles with some larger particles from the waste rock before the onset of pyrite oxidation and release of fully oxidized As. This flushing of As and Fe is a result of their association where As is commonly sorbed to Fe (oxyhydr)oxides [99]. Nanoparticle Fe (oxyhydr)oxides are common and have a high surface energy that will readily sorb other metal(loid)s such as As [14,100,101].

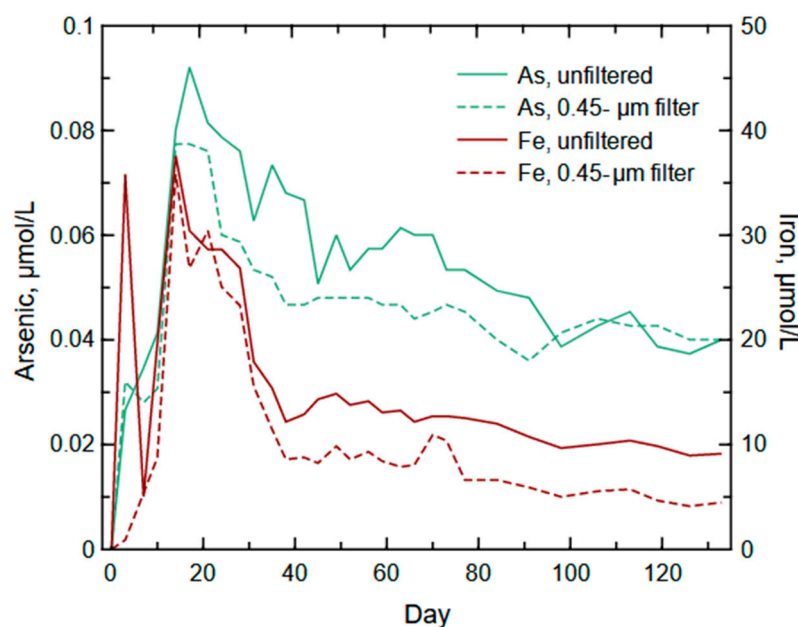


Figure 12. Unfiltered and 0.45- μm filtered iron and arsenic concentrations recorded during the column experiment.

The enhanced model (Figure 13) for As release incorporated the nanomaterial contribution (second source) through the dissolution of arsenolite [As_4O_6], an oxidation product of arsenic sulfide, to replicate nanoparticle desorption (initial concentration peak) to complement the As release from the oxidative dissolution of pyrite (second concentration peak from the primary source (basic model)). The arsenolite dissolution was set to a typical fast dissolving salt ($\log k = -12$) to replicate the quick release into solution. The enhanced modeled As release trend is similar to the filtered As release trend from the column experiment, although a larger release of As was present in the column experiment during the second peak. This additional mass of As in the filtered column water likely is the continued release of As-bearing particles moving through the low permeability waste rock (a 2-h drain period was necessary to capture drainable water from the approximate 0.5-m column of saturated waste rock). The removal of transportable particles from the column and reduction of the early availability of a substantial portion of pyrite surface area produced a post-Day 30 weathering trend representative of the slow release of As from pyrite oxidation as the available surface area was reduced.

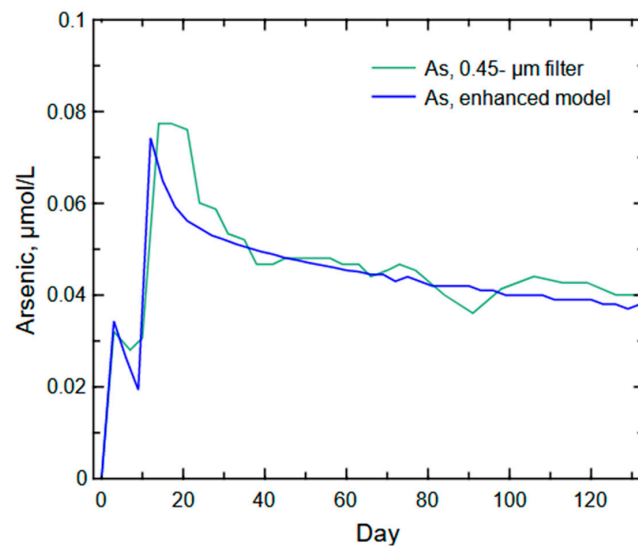


Figure 13. Arsenic concentrations predicted from the enhanced arsenic model of nanoparticle contribution and oxidative dissolution of arsenic-bearing pyrite compared to the column experiment's filtered (<450 μm) arsenic concentrations.

3.5. Initial Selenium Model vs. the Column Experiment

Analysis of Se in the unfiltered (total), 0.45- μm filtered, and 0.20- μm filtered column results indicate similar Se concentrations for all sample types. The presence of Se salts in the waste rock [35,69] and the results of the column experiment suggest that Se was present as Se ions or flushed from the waste rock as <0.20- μm nanomaterials. The column Se results indicated an initial spike in Se concentrations that quickly declined to very low concentrations by Day 10 and non-detectable levels by Day 17 (Figure 14). Such a quick Se release and decline are indicative of a fast mineral reaction (e.g., salt dissolution) and/or flushing of a nanomaterial source (e.g., desorption of selenite/selenate particles). Given the solubility of selenate, limited mobility of selenite, and oxygenated conditions recorded during the column experiment, Se likely was present as selenate derived from the oxidative dissolution of Se salts.

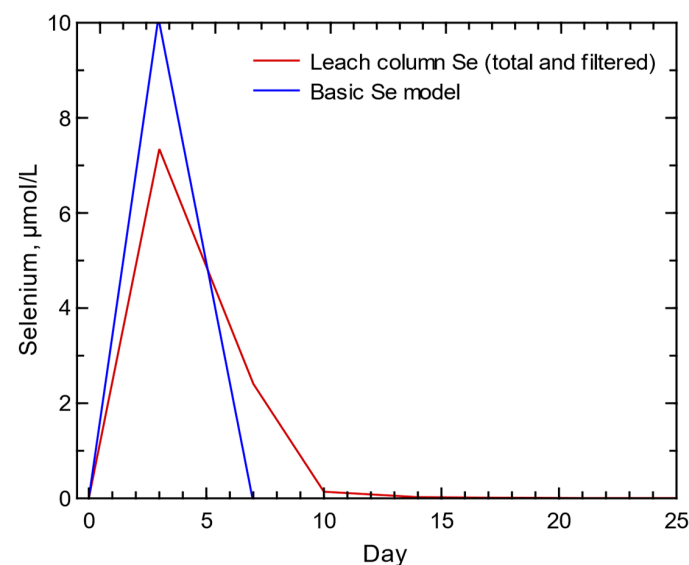


Figure 14. Selenium results for basic selenium model with dissolution of a selenium-bearing gypsum and total (unfiltered) and filtered selenium concentrations recorded during the column experiment. Selenium concentrations recorded from the column experiment were the same for the total, 0.45- μm filtered, and 0.2- μm filtered concentrations.

The initial Se model was based on the dissolution of a Se-bearing salt (95% gypsum + 5% nestolaite) given the presence of substantial gypsum in the waste rock formations and noticeably quick release of Se with weathering of the waste rock in the column experiment. The basic model of Se salt dissolution produced a similarly quick concentration peak comparable to the Se release from the column experiment, but the modeled Se trend indicated that all Se was quickly released, not the quick concentration peak and slower concentration decline visible in the column concentrations (Figure 14). This contrast in Se release trend is suggestive of a second, yet slightly slower, process of Se release from the waste rock that is necessary to account for the slower decline in concentrations visible in the column results.

3.6. Enhanced Selenium Model vs. the Column Experiment

The initial Se model identified the timing of the Se peak in the column results but not the post-peak decline of column concentrations (Figure 14). A model of salt dissolution and bulk solid Se-bearing pyrite would not replicate the column results but simply add to the peak concentration followed by a slower decline in concentrations, similar to the As-bearing pyrite oxidation and As release. An enhanced model of Se salt dissolution (part of peak concentration) and oxidation of Se-containing nanopyrite (surface-to-volume ratio of 4.2 but same log k of -8.19 for pyrite [86]) was able to replicate the column results (Figure 14). The enhanced model identified a peak concentration from salt dissolution and greater release of Se with oxidation of a nanopyrite that produced a near replication of the post-peak decline visible in the column experiment concentrations (Figure 15). An increase of the surface-to-volume ratio from the standard 0.3 value used for pyrite oxidation [86] represents a substantial increase in potential weathering applicable to nanomaterials generated during mining. Nanomaterials can be highly reactive because the area-to-volume ratio substantially increases as particle size decreases, which allows for a much greater available surface for reactions [102]. The change in particle size during waste rock generation should depend on the mineral type, composition, and original particle shape [10]. The identification of nanopyrite in coal mine waste rock [63] supports the inclusion of such reactive sources for potential contaminants, such as Se.

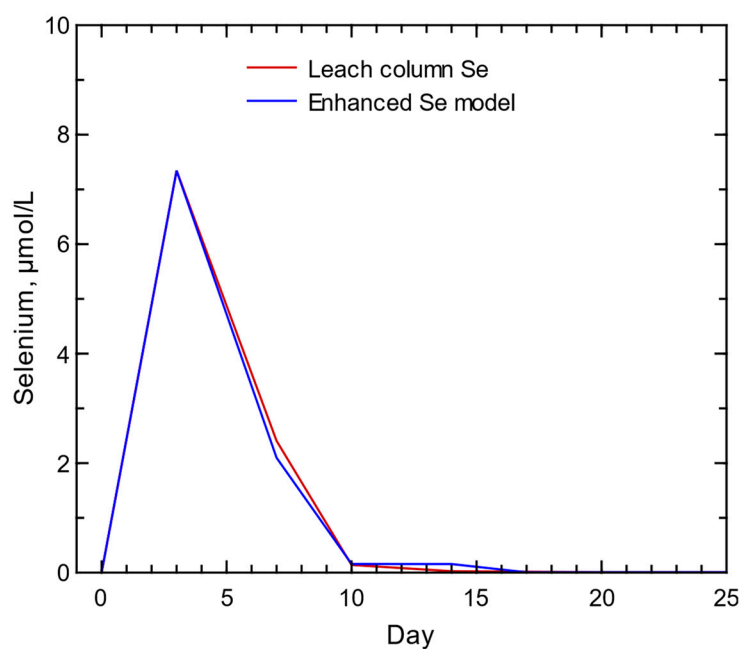


Figure 15. Selenium concentrations predicted from the enhanced selenium model of dissolution of selenium-bearing gypsum and selenium-bearing nanopyrite compared to the column experiment selenium concentrations (total and filtered selenium concentrations were identical during the column experiment).

4. Conclusions

The complexity of predicting the water quality of a backfill aquifer is a result of the change in the waste rock from its overburden state to its mined state. The alteration of the material with mining exposes previously bound mineral surfaces and generates very fine to ultrafine particles or nanomaterials. These newly available mineral surfaces and nanomaterials may contain contaminants that are now available for release in greater concentrations than predicted from the historical water chemistry of groundwater extracted from unmined overburden formations. Traditional geochemical modeling of known contaminant sources associated with overburden formations can capture the likely process(es) of mineral weathering and contaminant release, but additional source contributions from new mineral surfaces and nanomaterials likely are necessary to capture the high and variable solute load typically associated with the early weathering stage of fresh waste rock. The identification of such sources and potential water quality impacts may be difficult without characterization and weathering of the waste rock to identify these more reactive sources.

The release of arsenic and selenium from the weathering of coal mine waste rock in the Powder River Basin of Wyoming is not expected to be significant because of historical records that indicate the limited presence of these contaminants in groundwater extracted from the overburden formations. The column experiment with waste rock from the Cordero Rojo Mine in the Powder River Basin was evaluated for the temporal release of arsenic and selenium, which was compared to the release of these elements from basic predictive models. Each model produced a poor fit in comparison to the release of arsenic and selenium from the weathering experiment. Additional sources of each contaminant were added to the models to account for new reactive sources that allowed for the greater release of each element in the early weathering stage of the waste rock. The inclusion of the new sources produced near exact fits of the model outputs compared to the column experiment concentrations. It is unlikely that an arsenic or selenium kinetic model could have been developed that would have predicted the potential release of the elements without the results of the column experiment to guide the parameterization of the models. Therefore, predictive models for estimating potential water quality impacts in backfill aquifers require waste rock mineral and particle analysis to estimate potential new sources of contaminants made available during the mining process. Such an investigation will require not only characterization of the waste rock that is typically completed as part of the disposal process but solute characterization because of the greater availability of the potential contaminants in the waste rock state.

Supplementary Materials: The following supporting information can be downloaded at: <https://www.mdpi.com/article/10.3390/mining4030027/s1>.

Funding: This research received external funding from the U.S. Office of Surface Mining Reclamation and Enforcement under their Applied Science Program for Science and Technology Projects Related to Coal Mining and Reclamation (Grant# S21AC10037).

Data Availability Statement: Column experiment data analyzed as part of this study can be found at: <https://www.mdpi.com/article/10.3390/geosciences14010004/s1> (accessed on 31 January 2024).

Acknowledgments: The author wishes to thank the Office of Surface Mining Reclamation and Enforcement for their support and funding and the Navajo Transitional Energy Company and the Cordero Rojo Mine for their collaboration and assistance. The author would also like to thank Julianna Martin and Gaige Swanson for their work on this project.

Conflicts of Interest: The author declares no conflicts of interest.

References

- Koch, D.H. Predicting the Impact of Spoils on Ground-Water Quality. *Ground. Monit. Remed.* **1983**, *3*, 42–45. [\[CrossRef\]](#)
- Van Voast, W.A.; Reiten, J.C. *Ground-Water Changes near Montana Coal Mines*; Montana State University: Billings, MT, USA, 1990.
- McCullough, C.D.; Marchand, G.; Unseld, J. Mine Closure of Pit Lakes as Terminal Sinks: Best Available Practice When Options Are Limited? *Mine Water Environ.* **2013**, *32*, 302–313. [\[CrossRef\]](#)
- Petavratzi, E.; Kingman, S.; Lowndes, I. Particulates from Mining Operations: A Review of Sources, Effects and Regulations. *Miner. Eng.* **2005**, *18*, 1183–1199. [\[CrossRef\]](#)
- Molins, S.; Knabner, P. Multiscale Approaches in Reactive Transport Modeling. *Rev. Mineral. Geochem.* **2019**, *85*, 27–48. [\[CrossRef\]](#)
- Steeffel, C.I. Reactive Transport at the Crossroads. In *Reactive Transport in Natural and Engineered Systems*; De Gruyter: Berlin, Germany, 2020; pp. 1–26. ISBN 978-1-5015-1200-1.
- Corona Sánchez, J.E.; González Chávez, M.C.A.; Carrillo González, R.; Scheckel, K.; Tapia Maruri, D.; García Cue, J.L. Metal(Loid) Bioaccessibility of Atmospheric Particulate Matter from Mine Tailings at Zimapán, Mexico. *Environ. Sci. Pollut. Res.* **2021**, *28*, 19458–19472. [\[CrossRef\]](#) [\[PubMed\]](#)
- Schindler, M.; Santosh, M.; Dotto, G.; Silva, L.F.O.; Hochella, M.F. A Review on Pb-Bearing Nanoparticles, Particulate Matter and Colloids Released from Mining and Smelting Activities. *Gondwana Res.* **2022**, *110*, 330–346. [\[CrossRef\]](#)
- Hoy, R.; Ogle, K.; Taylor, M. Evaluation of Water Quality Conditions in Coal Mine Backfill in the Powder River Basin of Wyoming. *J. Am. Soc. Min. Reclam.* **2003**, 427–447. [\[CrossRef\]](#)
- Hochella, M.F., Jr.; Lower, S.K.; Maurice, P.A.; Penn, R.L.; Sahai, N.; Sparks, D.L.; Twining, B.S. Nanominerals, Mineral Nanoparticles, and Earth Systems. *Science* **2008**, *319*, 1631–1635. [\[CrossRef\]](#)
- Dosseto, A.; Turner, S.P.; Chappell, J. The Evolution of Weathering Profiles through Time: New Insights from Uranium-Series Isotopes. *Earth Planet. Sci. Lett.* **2008**, *274*, 359–371. [\[CrossRef\]](#)
- Kim, C.S.; Wilson, K.M.; Rytuba, J.J. Particle-Size Dependence on Metal(Loid) Distributions in Mine Wastes: Implications for Water Contamination and Human Exposure. *Appl. Geochem.* **2011**, *26*, 484–495. [\[CrossRef\]](#)
- Nordstrom, D.K. Sulfide Mineral Oxidation. In *Encyclopedia of Geobiology*; Reitner, J., Thiel, V., Eds.; Encyclopedia of Earth Sciences Series; Springer: Dordrecht, The Netherlands, 2011; pp. 856–858. ISBN 978-1-4020-9211-4.
- Hochella, M.F., Jr.; Mogk, D.W.; Ranville, J.; Allen, I.C.; Luther, G.W.; Marr, L.C.; McGrail, B.P.; Murayama, M.; Qafoku, N.P.; Rosso, K.M.; et al. Natural, Incidental, and Engineered Nanomaterials and Their Impacts on the Earth System. *Science* **2019**, *363*, aau8299. [\[CrossRef\]](#) [\[PubMed\]](#)
- Warrender, R.; Howell, R.; Prestia, A.; Barnes, A.; Mansanares, W.; Miller, M. The Application of Predictive Geochemical Modelling to Determine Backfill Requirements at Turquoise Ridge Joint Venture, Nevada. *Geochem. Explor. Environ. Anal.* **2012**, *12*, 339–347. [\[CrossRef\]](#)
- Huisamen, A.; Wolkersdorfer, C. Modelling the Hydrogeochemical Evolution of Mine Water in a Decommissioned Opencast Coal Mine. *Int. J. Coal Geol.* **2016**, *164*, 3–12. [\[CrossRef\]](#)
- Qi, W.; Huang, Y.; He, H.; Zhang, J.; Li, J.; Qiao, M. Potential Pollution of Groundwater by Dissolution and Release of Contaminants Due to Using Gangue for Backfilling. *Mine Water Environ.* **2019**, *38*, 281–293. [\[CrossRef\]](#)
- Langman, J.B.; Moore, M.L.; Ptacek, C.J.; Smith, L.; Sego, D.; Blowes, D.W. Diavik Waste Rock Project: Evolution of Mineral Weathering, Element Release, and Acid Generation and Neutralization during a Five-Year Humidity Cell Experiment. *Minerals* **2014**, *4*, 257–278. [\[CrossRef\]](#)
- Hawkins, J.W. Predictability of Surface Mine Spoil Hydrologic Properties in the Appalachian Plateau. *Groundwater* **2004**, *42*, 119–125. [\[CrossRef\]](#) [\[PubMed\]](#)
- Anderson, S.P.; Anderson, R.S.; Hinckley, E.-L.S.; Kelly, P.; Blum, A. Exploring Weathering and Regolith Transport Controls on Critical Zone Development with Models and Natural Experiments. *Appl. Geochem.* **2011**, *26*, S3–S5. [\[CrossRef\]](#)
- Ehlen, J. Above the Weathering Front: Contrasting Approaches to the Study and Classification of Weathered Mantle. *Geomorphology* **2005**, *67*, 7–21. [\[CrossRef\]](#)
- Wellen, C.C.; Shatilla, N.J.; Carey, S.K. Regional Scale Selenium Loading Associated with Surface Coal Mining, Elk Valley, British Columbia, Canada. *Sci. Total Environ.* **2015**, *532*, 791–802. [\[CrossRef\]](#)
- White, A.F.; Brantley, S.L. Chemical Weathering Rates of Silicate Minerals: An Overview. *Rev. Mineral. Geochem.* **1995**, *31*, 1–22.
- Yoo, K.; Mudd, S.M. Discrepancy between Mineral Residence Time and Soil Age: Implications for the Interpretation of Chemical Weathering Rates. *Geology* **2008**, *36*, 35–38. [\[CrossRef\]](#)
- Acero, P.; Ayora, C.; Carrera, J.; Saaltink, M.W.; Olivella, S. Multiphase Flow and Reactive Transport Model in Vadose Tailings. *Appl. Geochem.* **2009**, *24*, 1238–1250. [\[CrossRef\]](#)
- Woessner, W.W.; Andrews, C.B.; Osborne, T.J. The Impacts of Coal Strip Mining on the Hydrogeologic System of the Northern Great Plains: Case Study of Potential Impacts on the Northern Cheyenne Reservation. *J. Hydrol.* **1979**, *43*, 445–467. [\[CrossRef\]](#)
- St-Arnault, M.; Vriens, B.; Blaskovich, R.; Aranda, C.; Klein, B.; Ulrich Mayer, K.; Beckie, R.D. Geochemical and Mineralogical Assessment of Reactivity in a Full-Scale Heterogeneous Waste-Rock Pile. *Miner. Eng.* **2020**, *145*, 106089. [\[CrossRef\]](#)
- Langman, J.B.; Blowes, D.W.; Sinclair, S.A.; Krentz, A.; Amos, R.T.; Smith, L.J.D.; Pham, H.N.; Sego, D.C.; Smith, L. Early Evolution of Weathering and Sulfide Depletion of a Low-Sulfur, Granitic, Waste Rock in an Arctic Climate: A Laboratory and Field Site Comparison. *J. Geochem. Explor.* **2015**, *156*, 61–71. [\[CrossRef\]](#)

29. Langman, J.; Torso, K.; Moberly, J. Seasonal and Basinal Influences on the Formation and Transport of Dissolved Trace Metal Forms in a Mining-Impacted Riverine Environment. *Hydrology* **2018**, *5*, 35. [\[CrossRef\]](#)
30. Harrison, A.L.; Dipple, G.M.; Song, W.; Power, I.M.; Mayer, K.U.; Beinlich, A.; Sinton, D. Changes in Mineral Reactivity Driven by Pore Fluid Mobility in Partially Wetted Porous Media. *Chem. Geol.* **2017**, *463*, 1–11. [\[CrossRef\]](#)
31. Martin, J.; Langman, J.B. Leachate Experiments to Evaluate Weathering of Waste Rock for Backfill Aquifers in Restored Coal Mine Pits, Powder River Basin, USA. *Geosciences* **2024**, *14*, 4. [\[CrossRef\]](#)
32. Naftz, D.L.; Rice, J.A. Geochemical Processes Controlling Selenium in Ground Water after Mining, Powder River Basin, Wyoming, U.S.A. *Appl. Geochem.* **1989**, *4*, 565–575. [\[CrossRef\]](#)
33. Fogg, J.L.; Martin, M.W.; Daddow, P.B. *Geohydrology and Potential Effects of Coal Mining in 12 Coal-Lease Areas, Powder River Structural Basin, Northeastern Wyoming*; U.S. Geological Survey: Reston, VA, USA, 1991.
34. Lindner-Lunsford, J.B.; Wilson, J.F., Jr. *Shallow Ground Water in the Powder River Basin, Northeastern Wyoming—Description of Selected Publications, 1950–91, and Indications for Further Study*; Water-Resources Investigations Report 91–4067; U.S. Geological Survey: Reston, VA, USA, 1992.
35. Dreher, G.B.; Finkelman, R.B. Selenium Mobilization in a Surface Coal Mine, Powder River Basin, Wyoming, U.S.A. *Environ. Geol. Water Sci.* **1992**, *19*, 155–167. [\[CrossRef\]](#)
36. Patz, M.J.; Reddy, K.J.; Skinner, Q.D. Trace Elements in Coalbed Methane Produced Water Interacting with Semi-Arid Ephemeral Stream Channels. *Water. Air. Soil Pollut.* **2006**, *170*, 55–67. [\[CrossRef\]](#)
37. Yuretic, R.F.; Hickey, L.J.; Gregson, B.P.; Hsia, Y.L. Lacustrine Deposits in the Paleocene Fort Union Formation, Northern Bighorn Basin, Montana. *J. Sediment. Res.* **1984**, *54*, 836–852. [\[CrossRef\]](#)
38. Pocknall, D.T. Paleoenvironments and Age of the Wasatch Formation (Eocene), Powder River Basin, Wyoming. *PALAIOS* **1987**, *2*, 368–376. [\[CrossRef\]](#)
39. Lorenz, J.C.; Nadon, G.C. Braided-River Deposits in A Muddy Depositional Setting: The Molina Member of the Wasatch Formation (Paleogene), West-Central Colorado, U.S.A. *J. Sediment. Res.* **2002**, *72*, 376–385. [\[CrossRef\]](#)
40. Larson, L.R. *Ground-Water Quality in Wyoming*; Water-Resources Investigations Report 84–4034; U.S. Geological Survey: Reston, VA, USA, 1984.
41. Martin, L.J.; Naftz, D.L.; Lowham, H.W.; Rankl, J.G. *Cumulative Potential Hydrologic Impacts of Surface Coal Mining in the Eastern Powder River Structural Basin, Northeastern Wyoming*; Water-Resources Investigations Report 88–4046; U.S. Geological Survey: Reston, VA, USA, 1988.
42. Colman, S.M. Rock-Weathering Rates as Functions of Time. *Quat. Res.* **1981**, *15*, 250–264. [\[CrossRef\]](#)
43. Drever, J.I.; Clow, D.W. Weathering Rates in Catchments. In *Reviews in Mineralogy and Geochemistry*; White, A.F., Brantley, S.L., Eds.; Mineralogical Society of America: Washington, DC, USA, 1995; Volume 31, pp. 463–483.
44. Heffern, E.L.; Coates, D.A. Geologic History of Natural Coal-Bed Fires, Powder River Basin, USA. *Int. J. Coal Geol.* **2004**, *59*, 25–47. [\[CrossRef\]](#)
45. Luppens, J.A. *A Critical Review of Published Coal Quality Data from the Southwestern Part of the Powder River Basin, Wyoming*; U.S. Geological Survey: Reston, VA, USA, 2011.
46. McClurg, J.E. Peat Forming Wetlands and the Thick Powder River Basin Coals. In *39th Field Conference Guidebook*; Eastern Powder River Basin-Black Hills; Wyoming Geological Association: Casper, WY, USA, 1988; pp. 29–236.
47. Moore, T.A. The Effects of Clastic Sedimentation on Organic Facies Development within a Tertiary Subbituminous Coal Bed, Powder River Basin, Montana, U.S.A. *Int. J. Coal Geol.* **1991**, *18*, 187–209. [\[CrossRef\]](#)
48. Ellis, M.S. *Quality of Economically Extractable Coal Beds in the Gillette Coal Field as Compared with Other Tertiary Coal Beds in the Powder River Basin, Wyoming and Montana*; Open-File Report; U.S. Geological Survey: Reston, VA, USA, 2002.
49. See, R.B.; Reddy, K.J.; Vance, G.F.; Fadlemawla, A.A.; Blaylock, M.J. *Geochemical Processes and the Effects of Natural Organic Solutes on the Solubility of Selenium in Coal-Mine Backfill Samples from the Powder River Basin, Wyoming*; Water-Resources Investigations Report 95–4200; U.S. Geological Survey: Reston, VA, USA, 1995.
50. Reed, S.M.; Singh, R.N. Groundwater Recovery Problems Associated with Opencast Mine Backfills in the United Kingdom. *Int. J. Mine Water* **1986**, *5*, 47–73. [\[CrossRef\]](#)
51. Reddy, K.J.; Zhang, Z.; Vance, G.F. Selenite and Selenate Determination in Surface Coal Mine Backfill Ground Water. In *Proceedings of the 12th Annual National Meeting of the American Society for Surface Mining and Reclamation*, Gillette, WY, USA, 3–8 June 1995; pp. 237–245.
52. Vance, G.F.; See, R.B.; Reddy, K.J. Selenite Sorption by Coal Mine Backfill Materials in the Presence of Organic Solutes. In *Environmental Chemistry of Selenium*; Frankenberger, W.T., Engberg, R.A., Eds.; Marcel Dekker, Inc.: New York, NY, USA, 1998; pp. 259–280. ISBN 978-0-429-07812-5.
53. White, A.F.; Peterson, M.L. Role of Reactive-Surface-Area Characterization in Geochemical Kinetic Models. In *Chemical Modeling of Aqueous Systems II*; American Chemical Society: Washington, DC, USA, 1990; Volume 416, pp. 461–475. ISBN 0-8412-1729-7.
54. de Assis, T.A.; Araújo Reis, F.D.A. Dissolution of Minerals with Rough Surfaces. *Geochim. Cosmochim. Acta* **2018**, *228*, 27–41. [\[CrossRef\]](#)
55. Filella, M.; Buffle, J. Factors Controlling the Stability of Submicron Colloids in Natural Waters. In *Colloids in the Aquatic Environment*; Tadros, T.F., Gregory, J., Eds.; Elsevier: Oxford, UK, 1993; pp. 255–273. ISBN 978-1-85861-038-2.

56. Chorover, J.; Kretzschmar, R.; Garcia-Pichel, F.; Sparks, D.L. Soil Biogeochemical Processes within the Critical Zone. *Elements* **2007**, *3*, 321–326. [\[CrossRef\]](#)
57. Gilbert, B.; Ono, R.K.; Ching, K.A.; Kim, C.S. The Effects of Nanoparticle Aggregation Processes on Aggregate Structure and Metal Uptake. *J. Colloid Interface Sci.* **2009**, *339*, 285–295. [\[CrossRef\]](#) [\[PubMed\]](#)
58. Fischer, C.; Kurganskaya, I.; Schäfer, T.; Lüttge, A. Variability of Crystal Surface Reactivity: What Do We Know? *Appl. Geochem.* **2014**, *43*, 132–157. [\[CrossRef\]](#)
59. Kolker, A.; Palmer, C.A.; Bragg, L.J.; Bunnell, J.E. *Arsenic in Coal*; U.S. Geological Survey: Reston, VA, USA, 2005; p. 4.
60. Reich, M.; Becker, U. First-Principles Calculations of the Thermodynamic Mixing Properties of Arsenic Incorporation into Pyrite and Marcasite. *Chem. Geol.* **2006**, *225*, 278–290. [\[CrossRef\]](#)
61. Kipp, G.G.; Stone, J.J.; Stetler, L.D. Arsenic and Uranium Transport in Sediments near Abandoned Uranium Mines in Harding County, South Dakota. *Appl. Geochem.* **2009**, *24*, 2246–2255. [\[CrossRef\]](#)
62. Corkhill, C.L.; Vaughan, D.J. Arsenopyrite Oxidation—A Review. *Appl. Geochem.* **2009**, *24*, 2342–2361. [\[CrossRef\]](#)
63. Ribeiro, J.; Taffarel, S.R.; Sampaio, C.H.; Flores, D.; Silva, L.F.O. Mineral Speciation and Fate of Some Hazardous Contaminants in Coal Waste Pile from Anthracite Mining in Portugal. *Int. J. Coal Geol.* **2013**, *109–110*, 15–23. [\[CrossRef\]](#)
64. Oliveira, M.L.S.; Da Boit, K.; Schneider, I.L.; Teixeira, E.C.; Crissien Borrero, T.J.; Silva, L.F.O. Study of Coal Cleaning Rejects by FIB and Sample Preparation for HR-TEM: Mineral Surface Chemistry and Nanoparticle-Aggregation Control for Health Studies. *J. Clean. Prod.* **2018**, *188*, 662–669. [\[CrossRef\]](#)
65. Barringer, J.L.; Reilly, P.A. Arsenic in Groundwater: A Summary of Sources and the Biogeochemical and Hydrogeologic Factors Affecting Arsenic Occurrence and Mobility. In *Current Perspectives in Contaminant Hydrology and Water Resources Sustainability*; IntechOpen: Rijeka, Croatia, 2013; pp. 83–116. [\[CrossRef\]](#)
66. Neil, C.W.; Jason Todd, M.; Jeffrey Yang, Y. Improving Arsenopyrite Oxidation Rate Laws: Implications for Arsenic Mobilization during Aquifer Storage and Recovery (ASR). *Environ. Geochem. Health* **2018**, *40*, 2453–2464. [\[CrossRef\]](#) [\[PubMed\]](#)
67. Shamberger, R.J. Selenium in the Environment. *Sci. Total Environ.* **1981**, *17*, 59–74. [\[CrossRef\]](#)
68. McNeal, J.M.; Balistrieri, L.S. Geochemistry and Occurrence of Selenium: An Overview. In *Selenium in Agriculture and the Environment*; John Wiley & Sons, Ltd.: London, UK, 1989; pp. 1–13. ISBN 978-0-89118-918-3.
69. Yudovich, Y.E.; Ketris, M.P. Selenium in Coal: A Review. *Int. J. Coal Geol.* **2006**, *67*, 112–126. [\[CrossRef\]](#)
70. Sharmasarkar, S.; Vance, G.F. Fractional Partitioning for Assessing Solid-Phase Speciation and Geochemical Transformations of Soil Selenium. *Soil Sci.* **1995**, *160*, 43. [\[CrossRef\]](#)
71. Elrashidi, M.A.; Adriano, D.C.; Workman, S.M.; Lindsay, W.L. Chemical Equilibria of Selenium in Soils: A Theoretical Development. *Soil Sci.* **1987**, *144*, 141. [\[CrossRef\]](#)
72. Torres, J.; Pintos, V.; Domínguez, S.; Kremer, C.; Kremer, E. Selenite and Selenate Speciation in Natural Waters: Interaction with Divalent Metal Ions. *J. Solut. Chem.* **2010**, *39*, 1–10. [\[CrossRef\]](#)
73. Torres, J.; Pintos, V.; Gonzatto, L.; Domínguez, S.; Kremer, C.; Kremer, E. Selenium Chemical Speciation in Natural Waters: Protonation and Complexation Behavior of Selenite and Selenate in the Presence of Environmentally Relevant Cations. *Chem. Geol.* **2011**, *288*, 32–38. [\[CrossRef\]](#)
74. Paydary, P.; Schellenger, A.E.P.; Teli, M.; Jaisi, D.P.; Onnis-Hayden, A.; Larese-Casanova, P. Chemical Oxidation of Selenite to Selenate: Evaluation of Reactive Oxygen Species and O Transfer Pathways. *Chem. Geol.* **2021**, *575*, 120229. [\[CrossRef\]](#)
75. Lee, R.W. *Geochemistry of Water in the Fort Union Formation of the Northern Powder River Basin, Southeastern Montana*; Open-File Report 80–336; U.S. Geological Survey: Reston, VA, USA, 1980.
76. Huggins, F.E.; Huffman, G.P.; Lin, M.C. Observations on Low-Temperature Oxidation of Minerals in Bituminous Coals. *Int. J. Coal Geol.* **1983**, *3*, 157–182. [\[CrossRef\]](#)
77. Healy, R.W.; Rice, C.A.; Bartos, T.T.; McKinley, M.P. Infiltration from an Impoundment for Coal-Bed Natural Gas, Powder River Basin, Wyoming: Evolution of Water and Sediment Chemistry. *Water Resour. Res.* **2008**, *44*, W06424. [\[CrossRef\]](#)
78. Rice, C.A.; Flores, R.M.; Stricker, G.D.; Ellis, M.S. Chemical and Stable Isotopic Evidence for Water/Rock Interaction and Biogenic Origin of Coalbed Methane, Fort Union Formation, Powder River Basin, Wyoming and Montana U.S.A. *Int. J. Coal Geol.* **2008**, *76*, 76–85. [\[CrossRef\]](#)
79. American Society for Testing and Materials. *Practice for Sampling Aggregates*; ASTM International: West Conshohocken, PA, USA, 2019; p. 7.
80. American Society for Testing and Materials. *Practice for Probability Sampling of Materials*; ASTM International: West Conshohocken, PA, USA, 2016; p. 4.
81. Lapakko, K.A. Developments in Humidity-Cell Tests and Their Application. In *Environmental Aspects of Mine Wastes*; Mineralogical Association of Canada Short Course Series; Jambor, J.L., Blowes, D.W., Ritchie, A.I.M., Eds.; Economic Geology Publishing Company: New Haven, CT, USA, 2003; pp. 147–164.
82. Lapakko, K.A.; White, W.W. Modification of the ASTM 5744-96 Kinetic Test. In *Proceedings of the Fifth International Conference on Acid Rock Drainage*, Littleton, CO, USA, 20–26 May 2000; pp. 631–639.
83. American Society for Testing and Materials. *Test Method for Laboratory Weathering of Solid Materials Using a Humidity Cell*, ASTM D5744-18; ASTM International: West Conshohocken, PA, USA, 2018; p. 24.
84. American Society for Testing and Materials. *Standard Guide for Interpretation of Standard Humidity Cell Test Results*, ASTM D8187-18; ASTM International: West Conshohocken, PA, USA, 2018; p. 24.

85. Hunter, R.J. The Calculation of Zeta Potential. In *Zeta Potential in Colloid Science*; Academic Press: New York, NY, USA, 1981; pp. 59–124. ISBN 978-0-12-361961-7.
86. Williamson, M.A.; Rimstidt, J.D. The Kinetics and Electrochemical Rate-Determining Step of Aqueous Pyrite Oxidation. *Geochim. Cosmochim. Acta* **1994**, *58*, 5443–5454. [[CrossRef](#)]
87. Lapakko, K.A. Preoperational Assessment of Solute Release from Waste Rock at Proposed Mining Operations. *Appl. Geochem.* **2015**, *57*, 106–124. [[CrossRef](#)]
88. Lebedev, A.L. Kinetics of Gypsum Dissolution in Water. *Geochem. Int.* **2015**, *53*, 811–824. [[CrossRef](#)]
89. Drever, J.I.; Murphy, J.W.; Surdam, R.C. The Distribution of As, Be, Cd, Cu, Hg, Mo, Pb, and U Associated with the Wyodak Coal Seam, Powder River Basin, Wyoming. *Rocky Mt. Geol.* **1977**, *15*, 93–101.
90. Levenspiel, O. Experimental Search for a Simple Rate Equation to Describe Deactivating Porous Catalyst Particles. *J. Catal.* **1972**, *25*, 265–272. [[CrossRef](#)]
91. Davis, G.B.; Ritchie, A.I.M. A Model of Oxidation in Pyritic Mine Wastes: Part 1 Equations and Approximate Solution. *Appl. Math. Model.* **1986**, *10*, 314–322. [[CrossRef](#)]
92. Wunderly, M.D.; Blowes, D.W.; Frind, E.O.; Ptacek, C.J. Sulfide Mineral Oxidation and Subsequent Reactive Transport of Oxidation Products in Mine Tailings Impoundments: A Numerical Model. *Water Resour. Res.* **1996**, *32*, 3173–3187. [[CrossRef](#)]
93. Wilson, D.; Amos, R.T.; Blowes, D.W.; Langman, J.B.; Smith, L.; Sego, D.C. Diavik Waste Rock Project: Scale-Up of a Reactive Transport Model for Temperature and Sulfide-Content Dependent Geochemical Evolution of Waste Rock. *Appl. Geochem.* **2018**, *96*, 177–190. [[CrossRef](#)]
94. Wilson, D.; Amos, R.T.; Blowes, D.W.; Langman, J.B.; Ptacek, C.J.; Smith, L.; Sego, D.C. Diavik Waste Rock Project: A Conceptual Model for Temperature and Sulfide-Content Dependent Geochemical Evolution of Waste Rock—Laboratory Scale. *Appl. Geochem.* **2018**, *89*, 160–172. [[CrossRef](#)]
95. Hu, G.; Dam-Johansen, K.; Wedel, S.; Hansen, J.P. Decomposition and Oxidation of Pyrite. *Prog. Energy Combust. Sci.* **2006**, *32*, 295–314. [[CrossRef](#)]
96. Silva, J.C.M.; Santos, E.C.D.; Heine, T.; Abreu, H.A.D.; Duarte, H.A. Oxidation Mechanism of Arsenopyrite in the Presence of Water. *J. Phys. Chem. C* **2017**, *121*, 26887–26894. [[CrossRef](#)]
97. Cen, L.; Cheng, H.; Liu, Q.; Wang, S.; Wang, X. Arsenic Release from Arsenopyrite Weathering in Acid Mine Drainage: Kinetics, Transformation, and Effect of Biochar. *Environ. Int.* **2022**, *170*, 107558. [[CrossRef](#)]
98. Tabelin, C.B.; Corpuz, R.D.; Igarashi, T.; Villacorte-Tabelin, M.; Alorro, R.D.; Yoo, K.; Raval, S.; Ito, M.; Hiroyoshi, N. Acid Mine Drainage Formation and Arsenic Mobility under Strongly Acidic Conditions: Importance of Soluble Phases, Iron Oxyhydroxides/Oxides and Nature of Oxidation Layer on Pyrite. *J. Hazard. Mater.* **2020**, *399*, 122844. [[CrossRef](#)] [[PubMed](#)]
99. Bisone, S.; Chatain, V.; Blanc, D.; Gautier, M.; Bayard, R.; Sanchez, F.; Gourdon, R. Geochemical Characterization and Modeling of Arsenic Behavior in a Highly Contaminated Mining Soil. *Environ. Earth Sci.* **2016**, *75*, 306. [[CrossRef](#)]
100. Waychunas, G.A.; Kim, C.S.; Banfield, J.F. Nanoparticulate Iron Oxide Minerals in Soils and Sediments: Unique Properties and Contaminant Scavenging Mechanisms. *J. Nanopart. Res.* **2005**, *7*, 409–433. [[CrossRef](#)]
101. Navrotsky, A.; Mazeina, L.; Majzlan, J. Size-Driven Structural and Thermodynamic Complexity in Iron Oxides. *Science* **2008**, *319*, 1635–1638. [[CrossRef](#)] [[PubMed](#)]
102. Plathe, K.L.; von der Kammer, F.; Hassellöv, M.; Moore, J.N.; Murayama, M.; Hofmann, T.; Hochella, M.F., Jr. The Role of Nanominerals and Mineral Nanoparticles in the Transport of Toxic Trace Metals: Field-Flow Fractionation and Analytical TEM Analyses after Nanoparticle Isolation and Density Separation. *Geochim. Cosmochim. Acta* **2013**, *102*, 213–225. [[CrossRef](#)]

Disclaimer/Publisher’s Note: The statements, opinions and data contained in all publications are solely those of the individual author(s) and contributor(s) and not of MDPI and/or the editor(s). MDPI and/or the editor(s) disclaim responsibility for any injury to people or property resulting from any ideas, methods, instructions or products referred to in the content.